Mon. Not. R. Astron. Soc. **364,** 1239–1252 (2005) doi:10.1111/j.1365-2966.2005.09665.x

Stellar populations in a complete sample of local radio galaxies

D. Raimann,[1,2⋆] T. Storchi-Bergmann,[1⋆] H. Quintana,[3⋆] R. Hunstead[4⋆] and L. Wisotzki[5⋆]

[1]*Instituto de Física, Universidade Federal do Rio Grande do Sul, CP15051, Porto Alegre. 91501-970, RS, Brazil*
[2]*Universidade do Estado de Santa Catarina – CEO, Rua Aracajú s/n, Pinhalzinho, 89870-000, SC, Brazil*
[3]*Facultad de Física, Pontificia Universitad Catolica de Chile, Santiago, Chile*
[4]*School of Physics, University of Sydney, NSW 2006, Australia*
[5]*Astrophysikalisches Institut Potsdam, Potsdam, Germany*

Accepted 2005 September 25. Received 2005 September 1; in original form 2005 June 22

ABSTRACT

We investigate the nature of the continuum emission and stellar populations in the inner 1–3 kpc of a complete sample of 24 southern radio galaxies, and we compare the results with a control sample of 18 non-active early-type galaxies. 12 of the radio galaxies are classified as Fanaroff–Riley type I (FR I), eight as FR II and four as intermediate or undefined type (FR x). Optical long-slit spectra are used to perform spectral synthesis as a function of distance from the nucleus at an average sampling of 0.5–1.0 kpc and to quantify the relative contributions of a blue featureless continuum and stellar population components of different ages. Our main finding is a systematic difference between the stellar populations of the radio and control sample galaxies: the former have a larger contribution from an intermediate-age (1 Gyr) component, suggesting a connection between the present radio activity and a starburst which occurred ∼1 Gyr ago. In addition, we find a correlation between the contribution of the 1-Gyr component and the radio power, suggesting that more massive starbursts have led to more powerful radio emission. A similar relation is found between the radio power and the mean age of the stellar population, in the sense that stronger nuclear activity is found in younger galaxies.

We also find that the stellar populations of FR I galaxies are, on average, older and more homogeneous than those of FR IIs. Significant population gradients were found in only four radio galaxies, which are also those with more than 10 per cent of their total flux at 4020 Å contributed by age components younger than 100 Myr and/or a featureless continuum (indistinguishable from a 3-Myr-old stellar population).

Key words: galaxies: active – galaxies: nuclei – quasars: general – galaxies: stellar content.

1 INTRODUCTION

The nature of the ultraviolet–optical (UV–optical) continuum in radio galaxies has been the subject of a number of recent studies (Tadhunter, Dickson & Shaw 1996; Aretxaga et al. 2001; Tadhunter et al. 2002; Wills et al. 2002, 2004). While at low redshifts most radio galaxies seem to show stellar populations dominated in the UV–optical by old stars, at high redshifts there is a UV excess, frequently associated with structures that are aligned with the large-scale radio structures, the so-called 'alignment effect' (McCarthy et al. 1987; Tadhunter et al. 1996, and references therein).

Several hypotheses have been advanced to explain the alignment effect: episodes of recent star formation associated with the evolution of the host galaxies (Lilly & Longair 1984); star formation episodes triggered by the passage of radio jets through the interstellar medium (Rees 1989); and scattered light from a hidden quasar (Fabian 1989; Tadhunter, Fosbury & di Serego Alighieri 1989).

Using detailed spectropolarimetric observations, Tadhunter et al. (1996) demonstrated that the UV–optical continuum of the low-redshift radio galaxy 3C 321 has a multicomponent nature. At 3639 Å, an old stellar population (15 Gyr) contributes 34 per cent of the total flux, an intermediate-age population (1 Gyr) contributes another 34 per cent, a hidden quasar provides 22 per cent and a nebular continuum 10 per cent. More recently, Tadhunter et al. (2002) performed a similar study using a larger sample of 22 luminous radio galaxies at intermediate redshifts ($0.15 < z < 0.7$), mostly composed of Fanaroff & Riley (1974) class II (FR II) radio galaxies. All of these show a UV excess. These results emphasize the multicomponent nature of the UV continuum in radio galaxies: only ∼1/3 comes from a significant contribution of polarized light (scattered

⋆E-mail: raimann@if.ufrgs.br (DR); thaisa@if.ufrgs.br (TS-B); hquintana@astro.puc.cl (HQ); rwh@physics.usyd.edu.au (RH); lwisotzki@aip.de (LW)

light from a hidden quasar), and the polarization level is never larger than 10 per cent; at 3600 Å, the nebular continuum is present in all objects, with varying proportions of 3–40 per cent; direct active galactic nucleus (AGN) light makes a significant contribution in 40 per cent of the objects and a young/intermediate-age stellar population (from 0.1 to 2 Gyr) is significant in 15–50 per cent of the radio galaxies.

At lower redshifts, Aretxaga et al. (2001) and Wills et al. (2002, 2004) have found similar results. Aretxaga et al. studied the optical spectra of the nuclei of seven luminous nearby radio galaxies ($z < 0.08$), which mostly correspond to the FR II class. Three of these show a UV excess. One is a broad-line radio galaxy where the UV excess is mainly due to direct AGN light. In two cases, the blue spectrum is dominated by blue supergiant and/or giant stars with ages from 7 to 40 Myr. Wills et al. (2002) studied the optical spectra of nine FR II radio galaxies ($0.05 < z < 0.2$). Four galaxies display a UV excess, with one being a broad-line radio galaxy. In the other three, the UV excess is due to young and/or intermediate-age stellar populations (from 0.5 to 2 Gyr). The four radio galaxies without UV excess have stellar populations typical of elliptical galaxies. The contribution of the nebular continuum varies from 0 to 26 per cent of the total flux at 3660 Å. No significant contribution from polarized light was found. In a subsequent paper, Wills et al. (2004) performed a similar study on 12 low-luminosity FR I radio galaxies ($z < 0.2$), finding that three objects show UV excess, the main contribution being due to young and/or intermediate-age stars.

The studies so far available in the literature refer to samples dominated by FR II galaxies, except for that of Wills et al. (2004) which is constrained to FR I galaxies only. There are no previous studies including a control sample, only a few stellar population studies of early-type galaxies (e.g. Quintana et al. 1990).

The novelty of our present work is threefold, as follows.

(i) To minimize selection effects, we chose a sample limited in redshift and radio flux, which is complete in the sense that it comprises the closest most luminous radio galaxies. It contains both FR I and FR II radio galaxies.

(ii) We defined a control sample of early-type galaxies in order to look for systematic differences between the radio galaxies and non-active galaxies of similar Hubble types.

(iii) We extended the stellar population studies out to a few kpc from the nucleus, at a sampling of ∼0.2–1 kpc.

Our goal was to apply the technique we successfully used in previous studies of stellar populations of Seyfert, low-ionization nuclear emission-line region (LINER) and non-active galaxies (Cid Fernandes, Storchi-Bergmann & Schmitt 1998; Raimann et al. 2001, 2003; Raimann 2004) to address the following questions.

(i) What fraction of radio galaxies show a UV excess when compared with non-active galaxies of the same Hubble type?

(ii) What is the nature of this UV excess?

(iii) What fraction of radio galaxies exhibit signatures of recent star formation?

(iv) Are there systematic differences between the stellar population of FR I and FR II radio galaxies?

(v) Are there systematic differences between the stellar population of radio galaxies and non-active galaxies of the same Hubble type?

The paper is organized as follows. In Section 2 we describe the sample galaxies and the observations. In Section 3 we present the measurements of continuum colours, line equivalent widths and their radial variations. We describe the method and results of spectral synthesis in Section 4. In Section 5 we discuss the results, and in Section 6 we present our conclusions.

2 SAMPLE AND OBSERVATIONS

2.1 Radio galaxies

The sample of radio galaxies comprises 24 objects with $z < 0.08$ and integrated radio flux density $S(408\,\mathrm{MHz}) > 4.0$ Jy, extracted from the Molonglo Southern 4-Jy sample (Burgess & Hunstead 1994, 2005), with declinations in the range $-85^\circ < \delta < -30^\circ$ and galactic latitudes $|b| > 10^\circ$. The complete sample according to these criteria consists of 30 objects, but we could not observe six sources due to poor observational conditions. However, the exclusion of these sources does not seem to bias the survey or affect our conclusions.

In Table 1 we list the position, morphological type, radio classification (Fanaroff & Riley 1974), emission-line class (see below), apparent magnitude B, $S(408\,\mathrm{MHz})$, radial velocity cz and foreground galactic reddening $E(B-V)_{\mathrm{Gal}}$, for each galaxy. 12 radio galaxies are classified as FR I, eight are FR II and four are of intermediate or undefined type (FR x). The emission-line classes have been assigned according to the following criteria: BLRGs are radio galaxies with broad emission lines (i.e. permitted emission lines have both narrow- and broad-line components); NLRGs have narrow emission lines with equivalent widths $W_\lambda > 5$ Å; WLRGs are those with weak emission lines ($W_\lambda < 5$ Å); and NO-E have no emission lines. The radial velocities cz range from 8400 to 22 500 km s^{-1}, with a mean value of 15 000 km s^{-1} ($z \simeq 0.05$). The data were extracted from the NASA/IPAC Extragalactic Database (NED).

Long-slit spectra of these galaxies were obtained with the EMMI spectrograph at the 3.5-m New Technology Telescope (NTT) of the European Southern Observatory (ESO) at La Silla in 2001 September and 2002 February. The spectra were obtained in two segments, covering the wavelength ranges 3500–5000 and 4800–7300 Å, at spectral resolutions of 5 and 3.6 Å, respectively. Two exposures were obtained at each spectral region in order to eliminate cosmic rays, yielding total exposure times of 1800 s in the blue region and 3600 s in the red. The slit, with a width corresponding to 1.5 arcsec on the sky, was oriented along the major axis of the extended radio emission. The mean spatial scale is ∼1 kpc arcsec^{-1}. We present a log of the observations in Table 2.

The two-dimensional spectra were combined and reduced using standard tasks in IRAF (involving bias and flat-field correction, wavelength and flux calibration). One-dimensional spectra were extracted in windows of 1.5 arcsec in the bright nuclear regions and progressively larger windows towards the fainter outer regions. The red spectra were smoothed lightly to match the lower resolution of the blue spectra, after which the two segments were combined. Finally, the resulting spectra were corrected for foreground galactic extinction and shifted to the rest frame.

The spatial coverage ranges between 1 and 7 kpc at the galaxies (1.5–8 arcsec). The signal-to-noise (S/N) ratios of the extracted spectra range between 10 and 30. Representative spectra of the sample are shown in Fig. 1.

2.2 Control sample

The control sample comprises 18 non-active early-type galaxies: seven lenticulars and 11 ellipticals. These were selected to have similar Hubble types and absolute magnitudes to those of the radio galaxies, and no signs of nuclear activity. In order to be observable with a smaller telescope, the control sample galaxies were selected

Table 1. The radio galaxy sample.

Name	ID	α(2000)	δ (2000)	Morph.[a] type	FR[b] type	Emission type	B (mag)	S_{408} (Jy)	cz (km s^{-1})	$E(B-V)_{\rm Gal}$ (mag)
MRC B0023−333	ESO 350–G15	00 25 31	−33 02 46	E3	I	NO-E	14.6	4.1	14 940	0.015
MRC B0131−367	NGC 612	01 33 57	−36 29 35	SA0 pec	II	WLRG	13.5	17.1	8925	0.020
MRC B0214−480	ESO 198–G1	02 16 46	−47 49 23	E4	I	WLRG	15.0	5.5	19 190	0.023
MRC B0319−454	ESO 248–G10	03 21 08	−45 12 51	S	II	NLRG	15.6	8.3	18 887	0.015
MRC B0332−391	–	03 34 07	−39 00 03	E	I	NO-E	15.7	4.2	18 680	0.019
MRC B0344−345	–	03 46 30	−34 22 45	E	I/II	NLRG	16.2	7.6	16 130	0.012
MRC B0427−539	IC 2082	04 29 07	−53 49 39	–	I	WLRG	14.0	14.6	12 351	0.012
MRC B0429−616	–	04 30 22	−61 32 01	–	I	WLRG	15.5	4.4	16 680	0.022
MRC B0456−301	–	04 58 26	−30 07 22	E3	x	NLRG	17.5	7.2	18 900	0.013
MRC B0518−458	Pictor A	05 19 49	−45 46 44	(R')SA0 pec	II	BLRG	16.6	166.0	10 510	0.043
MRC B0618−371	ESO 365–IG6	06 20 00	−37 11 42	SAB0-:	II	NO-E	14.8	5.8	9838	0.080
MRC B0620−526	–	06 21 43	−52 41 36	–	I	WLRG	15.5	9.3	15 320	0.068
MRC B0625 − 536[c]	ESO 161–IG7	06 26 20	−53 41 33	E pec	I	NO-E	14.9	26.0	16 507	0.094
MRC B0715−362	–	07 17 08	−36 22 00	SA0-	I	NO-E	15.7	5.7	9593	0.282
MRC B1123−351	ESO 377–G46	11 25 52	−35 23 41	(R)SAB(rs)0	I	NO-E	14.0	6.6	10 119	0.087
MRC B1407−425	ESO 271–G20	14 10 28	−42 46 56	S	x	WLRG	15.1	4.7	15 889	0.081
MRC B1413−364	–	14 16 33	−36 40 54	E	II	NLRG	17.7	5.7	22 394	0.066
MRC B1637−771	–	16 44 16	−77 15 48	–	II	NLRG	16.3	13.5	12 801	0.099
MRC B1929−397	ESO 338–IG11	19 33 23	−39 40 23	–	II?	WLRG	15.5	4.3	22 504	0.152
MRC B2013−557	–	20 18 01	−55 39 30	E	I	NLRG	16.2	4.8	18 000	0.066
MRC B2148−555	–	21 51 29	−55 20 13	E2	I	NO-E	14.8	5.8	11 627	0.024
MRC B2152−699	ESO 075–G41	21 57 06	−69 41 23	SA0-	II	BLRG	14.1	61.6	8476	0.029
MRC B2158−380	AM 2158−380	22 01 17	−37 46 25	Sa	II	NLRG	14.8	4.1	9983	0.018
MRC B2354−350	ESO 349–G10	23 57 00	−34 45 30	E4	I	NLRG	14.0	8.7	14 705	0.013

[a]Galaxy morphology from the NED. [b]Radio type according to Fanaroff & Riley (1974). [c]Dumbbell galaxy; radio-source associated with eastern member.

to be closer ($z < 0.015$) than the radio galaxies. As we have not used any particular spectral characteristic to build this sample, we believe it is not biased, i.e. the conclusions of this work do not depend on the choice of these galaxies as control sample.

In Table 3 we list the positions, morphological types, apparent magnitudes B, radial velocities and foreground galactic reddening values of the control sample.

Long-slit spectra of the control sample were obtained mostly with the Boller & Chivens spectrograph at the 1.52-m telescope at the ESO. A few spectra were obtained with the Cassegrain spectrograph at the 4-m Blanco telescope at Cerro Tololo Inter-American Observatory and with the EMMI spectrograph at the 3.5-m NTT at the ESO. The wavelength range covered was 3600–7000 Å, at a spectral resolution of 4–6 Å. The slit, with a width corresponding to 1.5 arcsec on the sky, was oriented along the parallactic angle.

The galaxy NGC 4936 was observed with both the 1.52-m telescope and the NTT in order to check for any systematic differences in the spectra due to different instrumentation. We found none; the results of the measurements and population synthesis are identical for the two data sets within the errors. In order to illustrate this, we kept the entries corresponding to both observations of this galaxy in all the tables of the paper.

A log of these observations is presented in Table 4, where we list the exposure time, the slit position angle, the parallactic angle, airmass, spatial scale, telescope used and seeing. The mean spatial scale in the control sample is 0.16 kpc arcsec^{-1}, a factor of ∼6 smaller than for the radio galaxy sample.

Two or three exposures of each galaxy were obtained in order to eliminate cosmic rays. The two-dimensional spectra were combined and reduced using standard tasks in IRAF, as for the radio galaxy sample. One-dimensional spectra were extracted in windows of 1.5–3.2 arcsec in the bright nuclear regions and progressively larger windows towards the fainter outer regions.

The spatial coverage ranged between 0.15 and 4 kpc (3–36 arcsec) from the nucleus. The S/N ratio of the extracted spectra ranges between 10 and 30. Fig. 2 shows nuclear and extranuclear spectra of two representative galaxies of the control sample.

Note that the extraction samples smaller regions at the non-active galaxies than at the radio galaxies. Thus, whenever we compare the results for the radio galaxies with those for the control sample galaxies, we combine the nuclear and a few extranuclear extractions in the latter in order to cover similar spatial extents in the two samples (∼1 kpc).

3 EQUIVALENT WIDTHS OF ABSORPTION FEATURES AND CONTINUUM COLOURS

The analysis of the stellar population properties was performed using the same principles as in our previous papers (e.g. Raimann et al. 2001, 2003). We constructed a pseudo-continuum at selected pivot points of the spectra and measured the equivalent widths (W_λ) of eight absorption features. The pivot points for the continuum are at rest wavelengths 3660, 3780, 4020, 4510, 4630, 5313, 5870, 6080 and 6630 Å and the absorption features we measured are as follows: WLB (a blend of weak lines in the near-UV, within the spectral window λλ3810–3822), H9 (a blend of absorption lines which includes H9, window λλ3822–3858), Ca II K (λλ3908–3952), Ca II H+Hϵ (λλ3952–3988), the CN band (λλ4150–4214), the G band (λλ4284–4318), Mg I+MgH (λλ5156–5196) and Na I (λλ5880–5914).

Equivalent widths and continuum definitions are based on Bica & Alloin (1986), Bica (1988), Bica, Alloin & Schmitt (1994) and Raimann et al. (2001). The use of the same set of pivot points and wavelength windows allows a detailed quantitative analysis of the stellar populations via synthesis techniques, using the spectral library of star clusters of Bica & Alloin (1986) and Bica (1988).

Table 2. Observing log for the radio galaxies and spatial scale.

Name	PA[a] (°)	ψ [b] (°)	Airmass	Scale[c] (kpc arcsec^{-1})	Seeing (arcsec)	Linear[c,d] (kpc)	log L_{408}
ESO 350–G15	11	106	1.02	0.91	1.2	62	25.29
NGC 612	103	105	1.07	0.56	1.2	304	25.47
ESO 198–G1	173	148	1.07	1.15	1.2	490	25.63
ESO 248–G10	49	5	1.04	1.13	1.1	1745	25.80
MRC B0332−391	100	80	1.15	1.12	1.1	470	25.50
MRC B0344–345	105	92	1.13	0.98	1.5	265	25.62
IC 2082	109	71	1.26	0.76	1.2	210	25.64
MRC B0429−616	14	36	1.25	1.01	1.2	115	25.41
MRC B0456−301	103	83	1.14	1.13	1.0	395	25.73
Pictor A	102	82	1.35	0.65	1.0	283	26.57
ESO 365–IG6	88	110	1.05	0.61	1.0	60	25.07
MRC B0620−526	50	66	1.25	0.93	1.2	296	25.65
ESO 161–IG7	103	65	1.29	1.00	0.9	119	26.16
MRC B0715−362	82	90	1.22	0.60	0.7	269	25.04
ESO 377–G46	87	71	1.05	0.63	0.9	38	25.11
ESO 271–G20	102	117	1.18	0.96	1.2	47	25.40
MRC B1413−364	29	109	1.05	1.32	1.0	252	25.78
MRC B1637−771	0	40	1.60	0.79	1.4	206	25.66
ESO 338–IG11	134	157	1.02	1.33	0.7	150	25.66
MRC B2013−557	155	150	1.13	1.08	1.3	1300	25.52
MRC B2148−555	26	164	1.12	0.72	1.2	560	25.20
MRC ESO 075–G41	18	5	1.31	0.53	0.7	42	25.97
MRC AM 2158−380	40	140	1.03	0.62	1.2	71	24.93
MRC ESO 349–G10	141	123	1.01	0.90	1.4	61	25.59

[a]Slit position angle. [b]Parallactic angle. [c]Calculated for a flat *Wilkinson Microwave Anisotropy Probe* cosmology with $H_0 = 75$ km s^{-1} Mpc^{-1}. [d]Linear extent of the radio source.

3.1 Nuclear values

A summary of the nuclear measurements for the radio galaxies is presented in Table 5. This table lists the range of equivalent widths and continuum fluxes (relative to that at λ4020) measured in the nuclear spectra of the radio galaxies. The table also shows, for comparison, the corresponding values for the control sample. For the latter galaxies, nuclear and extranuclear spectra have been combined to cover a spatial extent ∼1 kpc, similar to that covered by the nuclear extractions of the radio galaxies. It can be seen that, while the upper limits for the two subsamples are similar, the radio galaxies have smaller W_λ on average, indicating the presence of an excess blue continuum. The radio galaxies must either have stellar populations younger or more metal-poor than those of the control sample, or nuclear spectra that are diluted by an AGN continuum.

The range of continuum fluxes is also broader in the radio sample, for which both bluer and redder continua are observed relative to the control sample.

3.2 Radial variations of equivalent widths and continuum colours

The variation of absorption-line equivalent widths and continuum colours as a function of distance from the nucleus allows us to study stellar population gradients. In non-active galaxies, the equivalent widths usually increase from the external regions towards the bulge, where they remain approximately constant. The presence of a burst of star formation and/or a featureless AGN continuum will produce a 'dilution' of the absorption lines, with a consequent decrease in equivalent width at the nucleus in comparison with values at adjacent locations (Cid Fernandes et al. 1998).

In Fig. 3 we illustrate the radial variations of W_λ, the continuum flux ratio F_{5870}/F_{4020} and the surface brightness at 4020 Å for two radio galaxies and two control sample galaxies of matched Hubble types. The dotted and dashed vertical lines mark distances at each galaxy of 1 and 3 kpc from the nucleus, respectively. The radio galaxy ESO 075–G41 shows dilution in most equivalent widths and has a bluer continuum at the nucleus than outside, while the radio galaxy MRC B0344−345 does not show dilution and has a redder nucleus than its surroundings. Some W_λ profiles show a decrease with distance from the nucleus. This latter behaviour is observed also in the control sample galaxies.

In our radio galaxy sample, only the two BLRGs, ESO 075–G41 and Pictor A, show clear dilutions of the nuclear equivalent widths and have a bluer nuclear continuum when compared with the extranuclear spectra. This dilution is thus probably due to the presence of a featureless continuum (hereafter FC) being directly observed in these galaxies. Most of the other radio galaxies do not show significant variation in W_λ along the slit, apart from a weak trend of decreasing W_λ away from the nucleus. The continuum is generally redder close to the nucleus than outside.

The non-active galaxies of the control sample also show little variation in equivalent width along the slit. Three of the lenticular galaxies from the control sample show stronger gradients, with nuclear equivalent widths ∼2 Å larger than at 1 kpc from the nucleus. In order to investigate whether the gradients were due to the proximity of these galaxies, thereby providing better spatial sampling, we binned several extracted spatial elements into one, in order to sample the same spatial extent as in the radio galaxies. Even after the binning, the gradients were still present. We thus concluded that the gradients are probably enhanced by the presence of the disc component in the lenticular galaxies. Regarding the continuum, only the

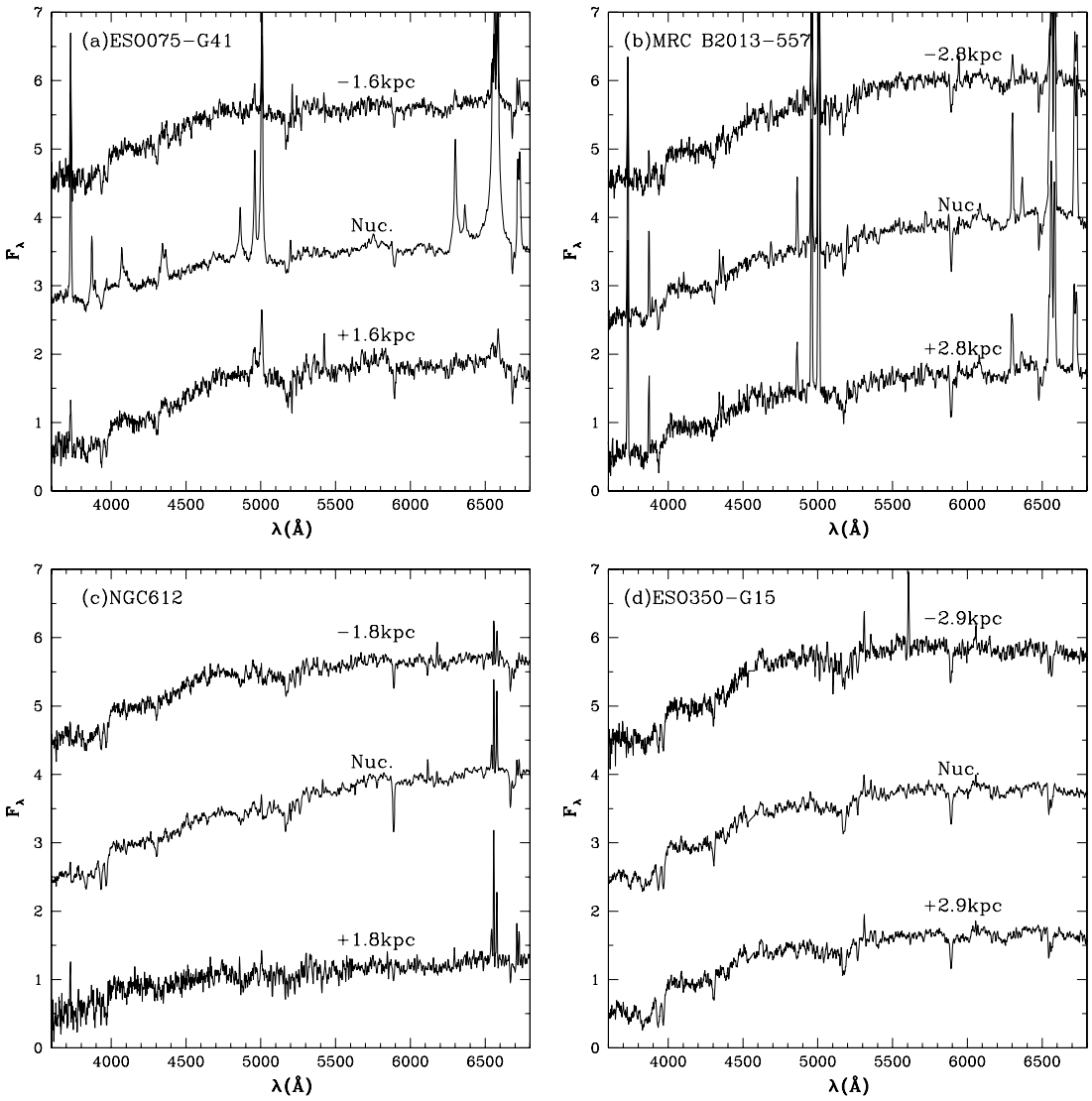

Figure 1. Sample of nuclear and extranuclear spectra of the radio galaxies: (a) BLRG; (b) NLRG; (c) WLRG; (d) radio galaxy without emission lines.

control galaxy NGC 2865 has a nuclear continuum bluer than in the extranuclear spectra; the others all have redder nuclear continua.

4 SPECTRAL SYNTHESIS

The spectral synthesis was performed using the probabilistic formalism described in Cid Fernandes et al. (2001). We reproduced the observed W_λ and continuum ratios (C_λ) using a base of star cluster spectra with different ages and metallicities (Bica & Alloin 1986). We used 12 components representing the age–metallicity plane plus a thirteenth component – the FC component – representing a canonical AGN continuum $F_\nu \propto \nu^{-1.5}$ (Schmitt, Storchi-Bergmann & Cid Fernandes 1999).

To synthesize the data from the two samples we used the continuum ratios $C_{3660} = F(3660)/F(4020)$, $C_{4510} = F(4510)/F(4020)$, $C_{5870} = F(5870)/F(4020)$ and $C_{6630} = F(6630)/F(4020)$, and the equivalent widths $W_{\rm WLB}$, $W_{\rm H9}$, $W_{\rm Ca\,II\,K}$, $W_{\rm CN\,band}$, $W_{\rm G\,band}$ and $W_{\rm Mg\,I+MgH}$. The adopted errors were $\sigma(W_\lambda) = 0.4$ Å for $W_{\rm Mg\,I+MgH}$, $\sigma(W_\lambda) = 0.5$ Å for $W_{\rm WLB}$, $W_{\rm H9}$, $W_{\rm Ca\,II\,K}$ and $W_{\rm G\,band}$, 1.0 Å for $W_{\rm CN\,band}$ and $\sigma(C_\lambda) = 0.05$ for the continuum ratios (Cid Fernandes et al. 1998). In a few cases the synthesis was performed with a smaller number of equivalent widths, due to contamination from emission lines.

As pointed out by Storchi-Bergmann et al. (2000) – see also Cid Fernandes et al. (2001) – it is not possible to discriminate the FC component from the 3-Myr young stellar component in this spectral range, for flux contributions smaller than 40 per cent at 4020 Å, because they have very similar continua. Therefore, in the description and discussion of the synthesis results we have combined the 3-Myr and FC components, which we refer to as the 3-Myr/FC component.

According to Cid Fernandes et al. (2001), this method of spectral synthesis can have difficulty in accurately determining the contributions of all 12 components of Bica's data base when the S/N ratio is modest or there are a reduced number of observables. These constraints act primarily in the sense of spreading a strong contribution in one component preferentially among base elements of different metallicities but of the same age. Therefore, in order to produce more robust results, we have grouped components of different metallicities but of the same age into one component, characterized

Table 3. The control sample.

Name	α(2000)	δ (2000)	Morph. type	B (mag)	cz (km s^{-1})	$E(B-V)_{\rm Gal}$ (mag)
NGC 1404	03 38 52	−35 35 37	E1	10.35	1497	0.011
NGC 1700	04 56 56	−04 51 55	E4	12.20	3895	0.043
NGC 2865	09 23 30	−23 09 43	E3-4	12.57	2627	0.082
NGC 3091	10 00 14	−19 38 13	E3:	12.13	3964	0.043
NGC 3585	11 13 17	−26 45 18	E7/S0	10.88	1399	0.064
NGC 3706	11 29 44	−36 23 33	SA(rs)0-	12.38	2977	0.092
NGC 3904	11 49 12	−29 16 35	E2-3:	11.83	1496	0.072
NGC 3923	11 51 01	−28 48 22	E4-5:	10.80	1788	0.083
NGC 4373	12 25 18	−39 45 37	SAB(rs)0-:	11.90	3396	0.080
NGC 4825	12 57 12	−13 39 53	SA(0)	12.63	4452	0.049
NGC 4936	13 04 17	−30 31 31	E0	11.77	3117	0.083
NGC 5061	13 18 04	−26 50 11	E0	11.44	2661	0.068
NGC 5328	13 52 53	−28 29 16	E1:	12.67	4740	0.062
NGC 5813	15 01 11	−01 42 08	E1-2	11.45	1972	0.057
NGC 6684	18 48 57	−65 10 26	(L)SB(r)0$^+$	11.31	847	0.067
NGC 6861	20 07 19	−48 22 12	SA(s)0	12.12	2819	0.054
NGC 7049	21 19 00	−48 33 43	SA(s)0	11.72	2231	0.007
NGC 7079	21 32 35	−44 04 00	(L)SB(r)0	12.46	2670	0.031

Table 4. Log of observations of the control sample.

Name	Exp. time (s)	PA (°)	ψ (°)	Airmass	kpc arcsec^{-1}	Telescope	Seeing (arcsec)
NGC 1404	5400	90	100	1.50	0.10	1.5-m ESO	0.8
NGC 1700	600	20	13	1.10	0.25	3.6-m NTT	1.5
NGC 2865	5400	90	36	1.02	0.17	1.5-m ESO	1.0
NGC 3091	5400	90	65	1.15	0.25	1.5-m ESO	0.9
NGC 3585	5400	90	150	1.01	0.09	1.5-m ESO	1.0
NGC 3706	5400	90	90	1.20	0.19	1.5-m ESO	0.9
NGC 3904	5400	90	81	1.19	0.10	1.5-m ESO	0.8
NGC 3923	5400	90	96	1.00	0.12	1.5-m ESO	0.8
NGC 4373	5400	90	20	1.02	0.21	1.5-m ESO	0.8
NGC 4825	5400	90	30	1.05	0.28	1.5-m ESO	0.9
NGC 4936	5400	90	90	1.01	0.19	1.5-m ESO	1.0
NGC 4936	600	86	86	1,07	0.19	3.6-m NTT	1.0
NGC 5061	5400	90	78	1.10	0.17	1.5-m ESO	0.9
NGC 5328	5400	90	95	1.10	0.30	1.5-m ESO	0.8
NGC 5813	600	90	30	1,25	0.13	3.6-m NTT	1.0
NGC 6684	1800	155	155	1.26	0.05	4-m CTIO	–
NGC 6861	1800	125	125	1.14	0.18	4-m CTIO	–
NGC 7049	1800	116	116	1.19	0.14	4-m CTIO	–
NGC 7079	5400	90	50	1.10	0.17	1.5-m ESO	1.5

by that age. We have thus neglected the potential differentiation in metallicity and concentrated on the more robust age information.

In Tables 6 and 7, we present the synthesis results as the relative contributions from components of four age bins to the total flux at 4020 Å: 10 Gyr, 1 Gyr, 100+10 Myr and 3-Myr/FC, in the nuclear region, at 1 and 3 kpc from the nucleus, respectively.

4.1 Synthesis results for the radio galaxies

The synthesis results for the radio galaxies are summarized in Table 6. In most of the radio galaxies, the nuclear and extranuclear stellar populations are dominated by old (10 Gyr) and intermediate-age (1 Gyr) components.

There are only four radio galaxies in which the younger or power-law components contribute more than 10 per cent of the total flux at 4020 Å, either at the nucleus or outside. Two of the latter galaxies are the BLRGs Pictor A and ESO 075–G41, in which the 3-Myr/FC component is probably dominated by the FC, as discussed in previous sections.

For the two BLRG galaxies, we performed another synthesis after subtracting the contribution of the 3-Myr/FC component, in order to test whether the underlying stellar population was similar to that in the other galaxies. We show the results of this new synthesis in parentheses in Table 6: the contribution of the 10-Gyr stellar population increases, indeed becoming more similar to that of the other galaxies, but the contribution of the 1-Gyr component does not, thus maintaining the difference from the other galaxies. There is an increase of the contribution of the 100+10 Myr component in the new synthesis. Finally, we point out that, for these galaxies, the

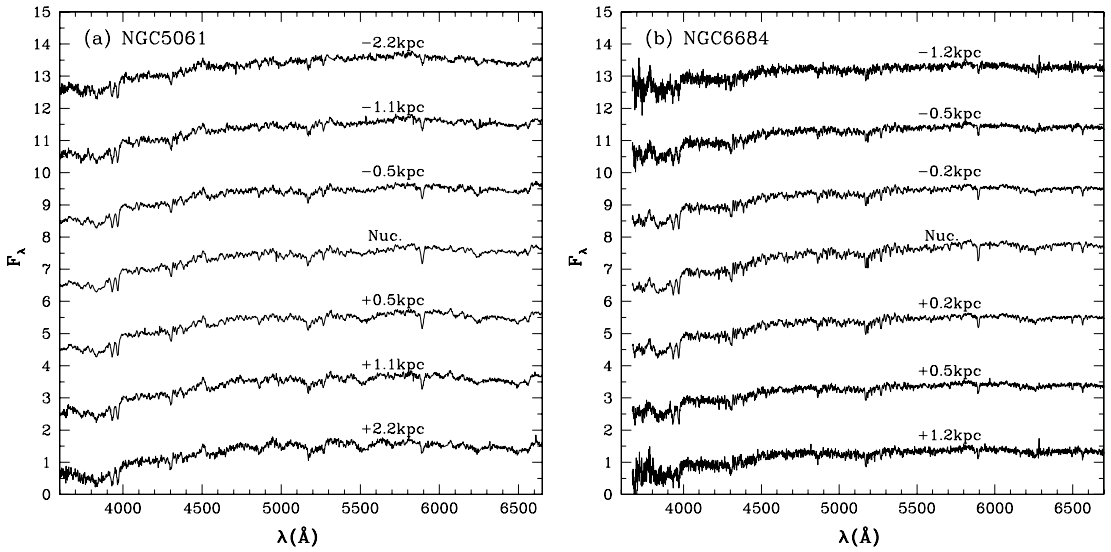

Figure 2. Spectra of (a) an elliptical and (b) a lenticular galaxy from the control sample.

Table 5. Range of nuclear equivalent widths and continuum fluxes from each subsample.

Sample	$W_{\rm WLB}$	$W_{\rm H9}$	$W_{\rm CaIIK}$	$W_{\rm CaIIH+H\epsilon}$	$W_{\rm CN}$	$W_{\rm G}$	$W_{\rm MgI+MgH}$	$W_{\rm NaI}$
Radio galaxies	1–7	7–18	8–20	8–15	5–15	4–12	4–11	4–9
Non-active galaxies	4–7	13–20	14–20	12–14	7–12	10–19	6–12	3–7
	3660 Å	4510 Å	5870 Å	6630 Å				
Radio galaxies	0.47–1.22	0.83–1.57	0.74–3.24	0.67–3.79				
Non-active galaxies	0.52–0.63	1.25–1.69	1.62–2.41	1.51–2.40				

synthesis results must be taken with caution, due to the fact that we have assumed a fixed slope for the power-law component (namely $F_\nu \propto \nu^{-1.5}$). As this component is very strong in these galaxies, if the real slope is different, it will affect the results of the synthesis. In particular, if the slope is harder than assumed, we may see excess blue light which could appear artificially as a large contribution of the 100+10 Myr component.

10-Gyr component

In 21 of the 24 radio galaxies the 10-Gyr component contributes from ∼50 to 70 per cent of the total flux in the nuclear region. The contribution is smaller only in MRC B0456–301 and in the two BLRGs before the subtraction of the 3-Myr/FC component. There is little variation with radius. Only five objects have differences between nuclear and extranuclear contributions larger than 10 per cent. In three cases the contribution of the 10-Gyr component decreases outwards and in the two BLRGs it increases, as expected. After subtraction of the 3-Myr/FC component from the spectra of the two BLRGs, the gradient disappears in Pictor A and is weakened in ESO 075–G41.

1-Gyr component

The 1-Gyr component contribution is dominant only in the nuclear spectrum of MRC B0456−301, and it contributes at least ∼30 per cent of the total flux in 19 objects. In four objects, the difference between nuclear and extranuclear contributions is ⩾10 per cent, with the contribution of this component increasing outwards.

Younger components

Besides the two BLRGs, the FR x galaxy MRC B0456–301 is the only radio galaxy which presents, at the nucleus and up to 1 kpc from it, a contribution of the 100+10 Myr component significantly larger than 10 per cent. NGC 612 displays such contribution at 3 kpc from the nucleus, probably triggered by an interaction related to its peculiar morphology. After subtracting the contribution of the 3-Myr/FC component from the spectra of Pictor A and ESO 075–G41, there is an increase of the contribution of the 100+10 Myr component.

Internal reddening

Internal reddening in the radio galaxies is generally small. The only cases of significant reddening, with values in the range $0.06 \leqslant E(B-V)_{\rm int} \leqslant 0.4$, are observed in the FR II/x galaxies NGC 612, ESO 248–G10, ESO 075–G41 and MRC B0344−345, and in the FR I galaxy MRC B2013−557.

Gradients

The 3-Myr/FC component decreases outwards in the two BLRGs but, as discussed above, this is most probably due to the unresolved FC component. By examining a stellar spatial profile, we concluded that at the angular distance corresponding to the galaxies to 1 kpc, there is still contamination of the spectra by a possible point source at the nucleus. This is the reason why, at 1 kpc, Table 6 shows some contribution from the 3-Myr/FC component. A true

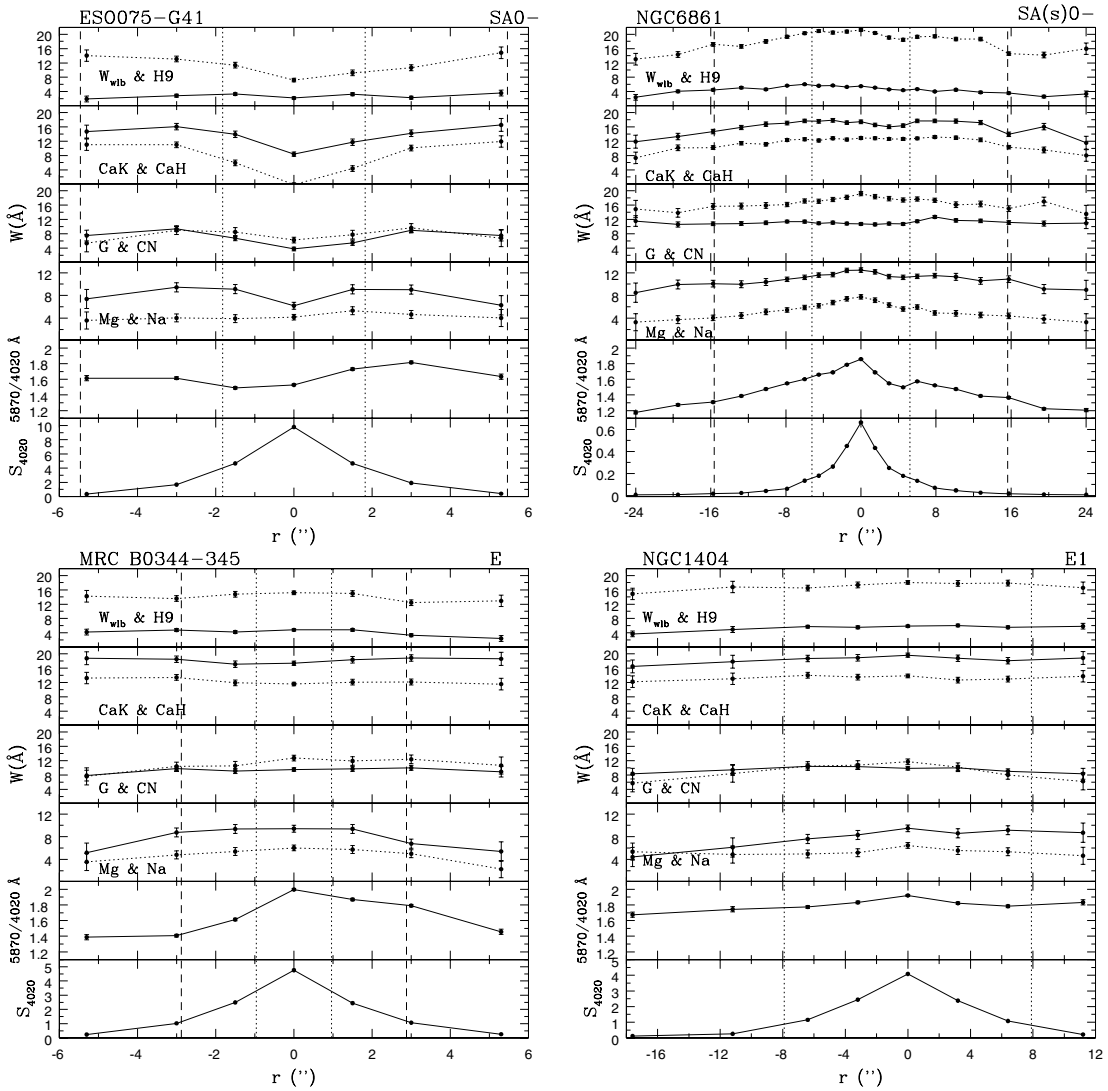

Figure 3. Radial variations of equivalent width, continuum colour and surface brightness for radio galaxies (top) and control sample galaxies (bottom). The first panel, from top to bottom, shows $W_{\rm WLB}$ (solid line) and $W_{\rm H9}$ (dotted), the second shows $W_{\rm Ca\,II K}$ (solid) and $W_{\rm Ca\,II H+H\epsilon}$ (dotted), the third shows $W_{\rm G\,band}$ (solid) and $W_{\rm CNband}$ (dotted), and the fourth shows $W_{\rm Mg\,I+MgH}$ (solid) and $W_{\rm Na\,I}$ (dotted). The fifth panel shows the continuum flux ratio between 5870 and 4020 Å. The sixth panel shows the run of the surface brightness at 4020 Å (in units of 10^{-15} erg cm^{-2} s^{-1} Å^{-1} arcsec^{-2}) along the slit. The dotted and dashed vertical lines mark distances of 1 and 3 kpc from the nucleus, respectively.

stellar population gradient is observed in the FR II galaxy NGC 612, in which the stellar population is predominantly old at the nucleus and there is a 100+10 Myr old component at a radius of 3 kpc.

4.2 Synthesis results for the control sample galaxies

The synthesis results for the control sample galaxies are summarized in Table 7.

10-Gyr component

The nuclear and extranuclear stellar populations of the non-active galaxies are dominated by the old (10 Gyr) component, which in most cases contributes 70–85 per cent of the total flux at 4020 Å.

1-Gyr component

The intermediate-age (1 Gyr) component is also significant in this sample and its contribution in most cases is within the range 15–30 per cent.

Younger age components

There are three non-active galaxies in which the 100+10 Myr component contributes 10 per cent or more of total flux at 4020 Å, but this contribution is never larger than 20 per cent. These three galaxies are ellipticals. The 3-Myr/FC component contribution is not significant in any of the galaxies of the control sample.

Reddening

None of the control sample galaxies shows internal reddening larger than $E(B-V)_{\rm int} = 0.05$.

Gradients

In general, we do not observe any population gradients in the galaxies of the control sample. Only three lenticular galaxies show

Table 6. Percentage contributions of four age bins to the total flux at 4020 Å for the radio galaxy sample, separated according to their FR classification.

Name	10 Gyr			1 Gyr			100+10 Myr			3-Myr/FC			Mean age
	Nuc.	1 kpc	3 kpc	Nuc.	1 kpc	3 kpc	Nuc.	1 kpc	3 kpc	Nuc.	1 kpc	3 kpc	(Gyr)
FR I													
ESO 350–G15	56	57	55	41	41	39	3	2	5	0	0	1	3.4
ESO 198–G1	53	54	51	44	43	46	3	3	2	0	0	1	3.2
MRC B0332−391	64	61	56	30	33	34	5	5	9	1	1	1	3.2
IC 2082	60	54	65	38	44	33	2	2	2	0	0	0	3.8
MRC B0429−616	50	50	53	42	43	39	7	6	7	1	1	1	2.2
MRC B0620−526	47	46	45	46	48	54	6	5	1	1	1	0	2.1
ESO 161–IG7	59	58	53	38	38	43	3	3	4	0	1	0	3.6
MRC B0715−362	72	61	–	17	33	–	9	5	–	2	1	–	2.8
ESO 377–G46	62	59	–	35	40	–	2	1	–	1	0	–	3.2
MRC B2013−557	49	46	33	42	46	61	7	6	4	2	1	2	1.7
MRC B2148−555	62	64	61	35	33	33	3	3	4	0	0	2	3.9
ESO 349–G10	61	62	59	35	33	36	3	4	4	1	1	1	3.1
FR II													
NGC 612	68	67	60	21	22	16	9	9	21	2	2	2	2.6
ESO 248–G10	52	47	47	44	49	47	3	3	5	1	1	1	2.5
Pictor A	21(45)	49	–	10(14)	8	–	12(41)	8	–	57	35	–	(1.1)
ESO 365–IG6	69	68	–	28	29	–	3	3	–	0	0	–	4.6
MRC B1413−364	63	52	–	33	43	–	3	4	–	1	1	–	3.2
MRC B1637−771	46	50	48	46	43	44	7	6	7	1	1	1	2.0
ESO 075–G41	39(55)	46	80	10(13)	23	11	24(32)	15	7	27	16	2	(1.7)
AM 2158−380	69	74	70	25	19	22	4	5	6	2	2	2	3.0
FR x													
MRC B0344−345	63	61	54	29	32	44	6	6	1	2	1	1	2.5
MRC B0456−301	14	13	–	60	51	–	24	31	–	2	5	–	0.5
ESO 271–G20	61	54	56	36	44	41	2	2	2	1	0	0	3.2
ESO 338–IG11	49	50	51	48	48	47	2	2	2	1	0	0	2.4

Table 7. Percentage contributions of four age bins to the total flux at 4020 Å for elliptical and lenticular galaxies from the control sample.

Name	10 Gyr			1 Gyr			100+10 Myr			3-Myr/FC		
	Nuc.	1 kpc	3 kpc	Nuc.	1 kpc	3 kpc	Nuc.	1 kpc	3 kpc	Nuc.	1 kpc	3 kpc
Ellipticals												
NGC 1404	75	79	–	22	16	–	3	5	–	0	0	–
NGC 1700	71	71	–	22	25	–	6	3	–	1	1	–
NGC 2865	56	65	–	24	19	–	20	15	–	0	1	–
NGC 3091	76	74	–	15	22	–	8	4	–	1	0	–
NGC 3585	73	82	–	20	14	–	6	4	–	1	0	–
NGC 3904	81	78	–	15	20	–	3	2	–	1	0	–
NGC 3923	69	77	–	25	19	–	6	4	–	0	0	–
NGC 4936[a]	75	88	–	19	10	–	4	2	–	2	0	–
NGC 4936[b]	81	80	–	11	16	–	6	3	–	2	1	–
NGC 5061	70	77	–	18	16	–	12	6	–	0	1	–
NGC 5328	66	67	–	24	18	–	9	14	–	1	1	–
NGC 5813	83	–	–	8	–	–	7	–	–	2	–	–
Lenticulars												
NGC 3706	78	76	–	12	19	–	8	4	–	2	1	–
NGC 4373	66	68	–	30	26	–	4	5	–	0	1	–
NGC 4825	80	81	79	12	12	11	7	6	6	1	1	3
NGC 6684	66	54	–	32	43	–	2	3	–	0	0	–
NGC 6861	67	53	37	27	44	53	6	3	10	0	0	0
NGC 7049	73	56	34	21	42	62	6	2	3	0	0	1
NGC 7079	50	45	–	48	52	–	2	3	–	0	0	–

[a]1.5-m ESO. [b]3.6-m NTT.

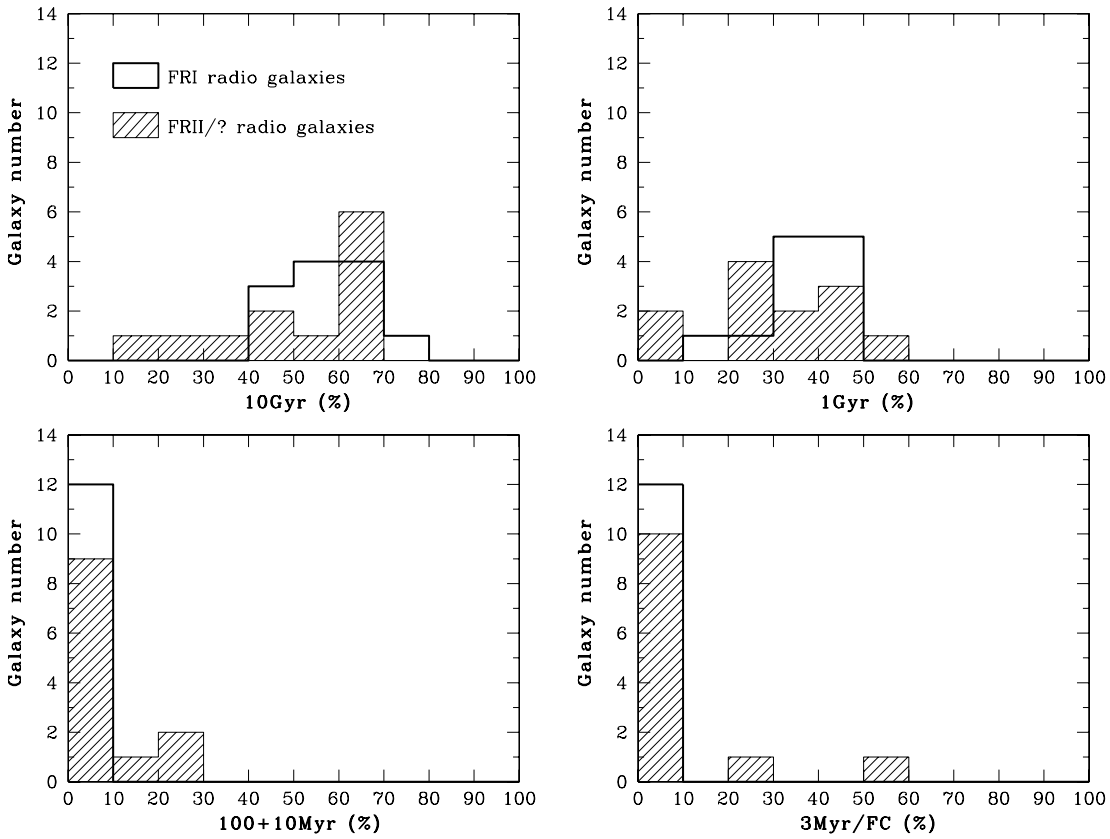

Figure 4. Histograms for the radio galaxies showing the contributions of different age components (10 Gyr, 1 Gyr, 100+10 Myr and 3-Myr/FC) to the total flux at 4020 Å. FR I galaxies are shown as open histograms with a heavy outline and FR II/x are shown hatched.

Table 8. The mean per cent contribution (and corresponding standard deviation) to the total flux at 4020 Å for the nuclear stellar populations of the 10-Gyr, 1-Gyr, 100+10 Myr and 3-Myr/FC components.

Objects	10 Gyr	1 Gyr	100+10 Myr	3-Myr/FC
FR I radio galaxies	57.9 (6.9)	36.9 (7.4)	4.4 (2.2)	0.8 (0.7)
FR II/x radio galaxies	51.2 (17.7)	32.5 (14.6)	8.3 (7.6)	8.1 (16.4)
All radio galaxies	54.5 (13.9)	34.7 (11.8)	6.3 (5.9)	4.4 (12.2)
Control sample	65.4 (17.3)	24.9 (11.1)	5.4 (4.1)	0.6 (0.6)

differences between the nuclear and extranuclear age components at a level greater than 10 per cent. In these three cases, the 10-Gyr component contribution decreases while the 1-Gyr contribution increases outwards. We attribute these gradients to the presence of a disc component in these galaxies, as discussed in Section 3.2.

5 DISCUSSION

5.1 Comparison of FR I versus FR II galaxies

In Fig. 4 we compare the population synthesis results of the FR I galaxies with those of the FR IIs, plus intermediate and uncertain types, for each age component. In each histogram, we show the number of galaxies as a function of the percentage contribution of that age component to the total flux at 4020 Å. We show the results only for the nucleus because we did not find significant spatial variation, as discussed in the previous sections. In Table 8 we list the mean per cent contribution of each age bin to the total flux at 4020 Å and the corresponding standard deviations.

The histograms show that the fractional contributions of each age component have a narrower distribution in FR I than in FR II galaxies. In other words, the stellar populations in FR I galaxies are more homogeneous than in FR II galaxies. No FR I galaxy has more than a 10 per cent contribution from components of age 100 Myr or younger, while four FR II/x galaxies have such components.

The above results translate into mean contributions (Table 8) of the 10- and 1-Gyr age components slightly larger in FR I than in FR II galaxies, while the reverse is true for the 100-Myr and younger components. The standard deviations are larger for FR II galaxies in accordance with their broader distributions in Fig. 4.

5.2 Relation with emission-line properties

Fig. 5 shows the distribution of fractional contributions of the four age components to the spectra of the radio galaxies where they are identified according to their emission-line spectra (BLRG, NLRG, WLRG and NO-E). The NO-E radio galaxies tend to have the largest contribution from the 10-Gyr stellar component (>50 per cent), similar to that of the control sample (see Section 5.4). The smallest contribution (<40 per cent) of the 10-Gyr component is observed in the two BLRGs and in the NLRG MRC B0456−301. Most of the NLRGs and WLRGs show intermediate values (40–70 per cent) for contributions of the 10-Gyr component. Regarding the 1-Gyr component, the only clear trend is that the BLRGs have the smallest contributions (<10 per cent). In the case of the 10 + 100 Myr age

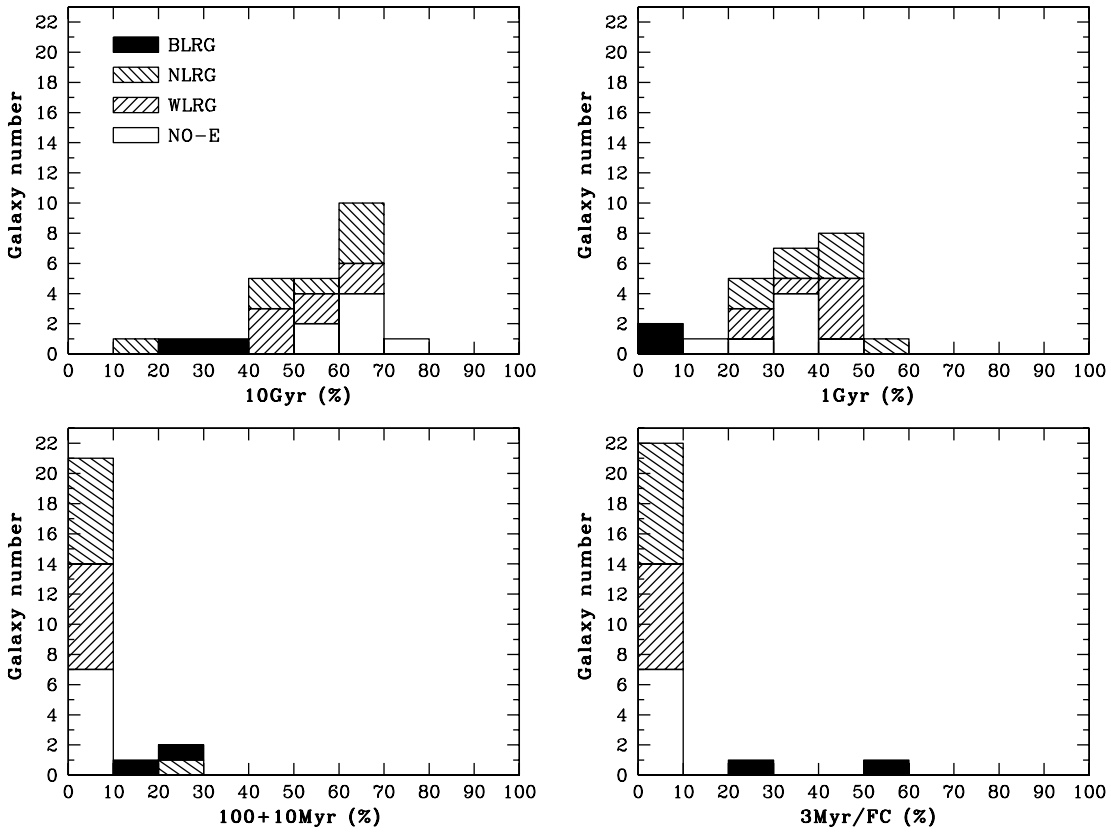

Figure 5. As in Fig. 4 for the radio galaxies identified according to their emission-line spectra: BLRG, NLRG, WLRG and NO-E.

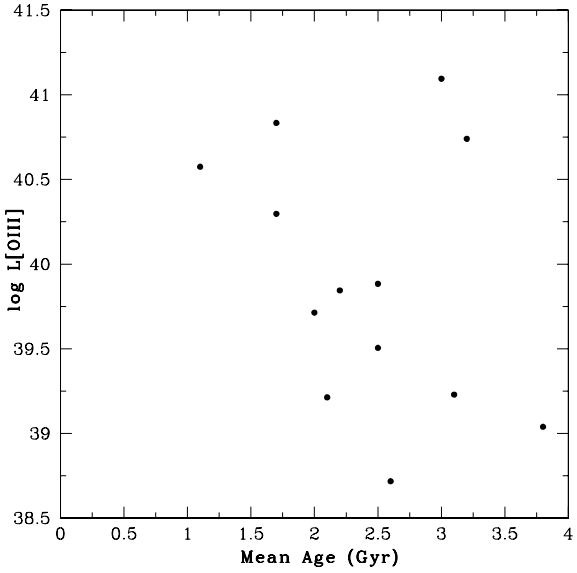

Figure 6. Relation between the luminosity $\log L_{[\mathrm{O\,III}]}$ and the mean age, as defined in the text.

component, the only three galaxies with a contribution larger than 10 per cent are the two BLRGs and one NLRG (MRC B0456−301); these are the same three galaxies which show the smallest contribution of the 10-Gyr component. In the case of the 3-Myr/FC component, only the two BLRGs show contributions larger than 10 per cent, which, as noted earlier, we attribute mostly to the FC.

In 13 radio galaxies we were able to measure the flux of the [O III] λ5007 emission line. In order to investigate the relation between the luminosity $L_{[\mathrm{O\,III}]}$ in this line and the age of the stellar population, we defined a percentage-weighted 'mean age' $\bar{t}$ as the mean decimal logarithm of the stellar population ages used in the synthesis, as follows:

$$\log(\bar{t}) \equiv \sum x_i \log(t_i). \quad (1)$$

For the four ages used here, this becomes (in yr)

$$\log(\bar{t}) \equiv 10x_{10} + 9x_9 + 8x_8 + 7x_7, \quad (2)$$

where x_i are the fractional contributions to the total flux at 4020 Å of the components with ages $t_i = 10^{10}$, 10^9, 10^8 and 10^7 yr. The values of $\bar{t}$ are listed in the last column of Table 6. For the two BLRGs, we calculated $\bar{t}$ excluding the 3-Myr/FC component.

The relation between $\log(L_{[\mathrm{O\,III}]})$ and $\log(\bar{t})$ can be seen in Fig. 6 for the nuclear spectra. Although the age spread is not large, there is a tendency for younger galaxies to have higher emission-line luminosities, while older galaxies seem to have a larger spread in their emission-line luminosities.

5.3 Relation with radio power

Although the radio luminosities do not cover a wide range, we also find some correlation between the radio power and the stellar populations properties of the radio galaxies. We have separated the radio sample into four power bins: <2, 2–4, 4–6 and >6 × 10^{25} W Hz^{-1}. The values of radio power are listed in the last column of Table 2. The distribution of the fractional contributions of the four age components split by radio power is shown in Fig. 7. The galaxies with

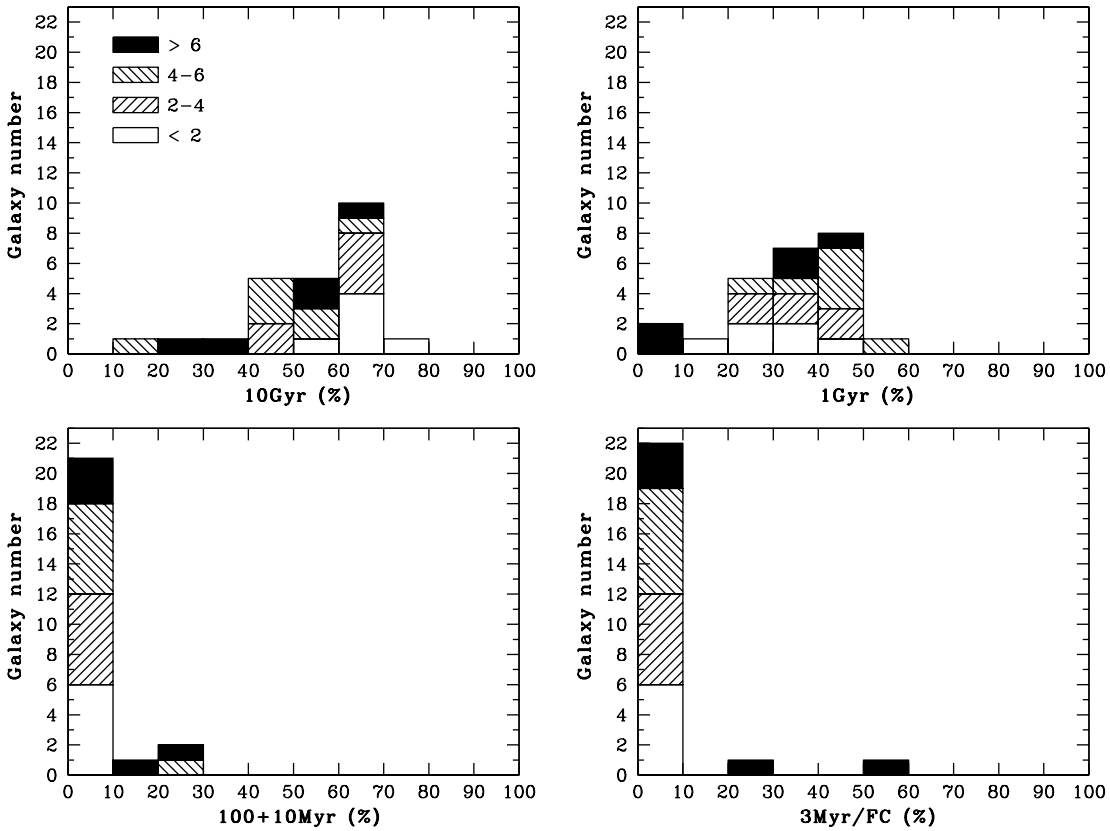

Figure 7. As in Fig. 4 for the radio galaxies identified as a function of radio power (in units of 10^{25} W Hz^{-1}).

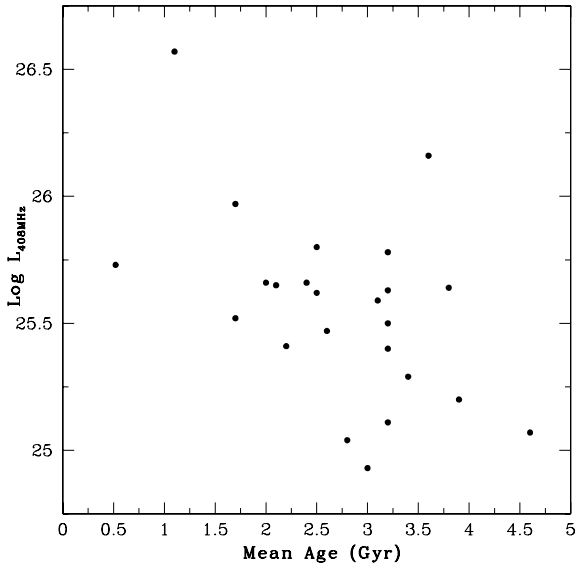

Figure 8. Relation between the log radio power (in units of W Hz^{-1}) and the mean age, as defined in the text.

lowest radio power tend to have the largest contribution from the 10-Gyr age component, and to have a stellar population mix closest to that of the control sample (see Section 5.4). For high radio power, the stellar population properties vary widely.

In order to better quantify the relation between the radio power and the age of the stellar population, we have plotted in Fig. 8 the logarithm of the radio luminosity at 408 MHz, log ($L_{408\,\mathrm{MHz}}$) against the mean age as calculated in the previous section. We observe an inverse relation in Fig. 8: the most powerful radio sources tend to be found in the youngest galaxies.

In Fig. 9 we show the percentage contribution of each age bin to the total flux at λ4020 against log ($L_{408\,\mathrm{MHz}}$). For most of the sample, there is an inverse relation between the contribution of the 10-Gyr component and the radio power: the most radio luminous galaxies present the smallest contribution of the 10-Gyr component. Only one galaxy does not follow the relation, MRC B0456–301, whose nuclear light is dominated by the contribution of the 1-Gyr and 100+10 Myr components.

There is also a direct relation between the contribution of the 1-Gyr component and radio power: larger radio power corresponds to larger contribution of the 1-Gyr component. The two BLRGs seem to be exceptions to this relation. Nevertheless, as pointed out in Section 4.1, the synthesis in these two cases may be uncertain due to the large contribution of the direct AGN light to the spectrum.

There is no obvious correlation of radio power with the younger age components.

5.4 Radio galaxies versus control sample

Fig. 10 shows comparative histograms for the radio galaxies and control sample galaxies in the percentage contributions of each age component to the flux at 4020 Å of the nuclear spectra. In the lower half of Table 8 we list the mean contributions and corresponding standard deviations.

The histograms and Table 8 show that the main differences between the stellar populations of the radio galaxies and control sample are in the relative contributions of the 10- and 1-Gyr components. In the radio galaxies, the contribution of the 10-Gyr component is

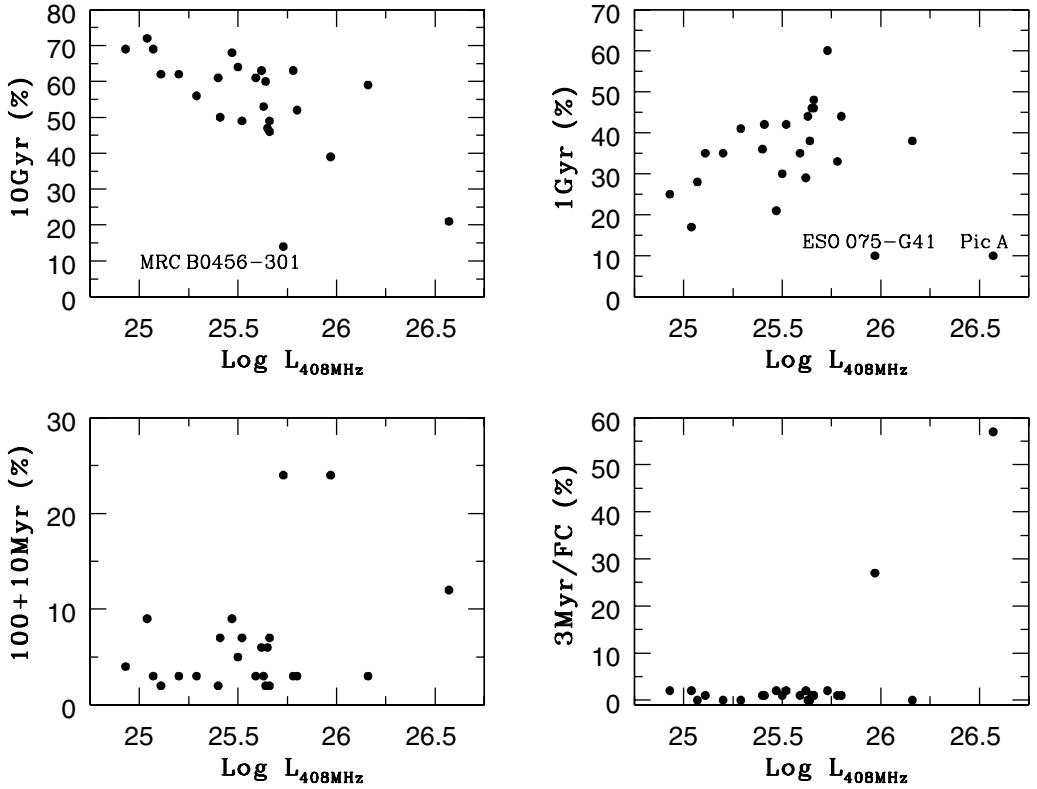

Figure 9. Fractional contribution (in per cent) of the different age components plotted against log radio power (in units W Hz^{-1}).

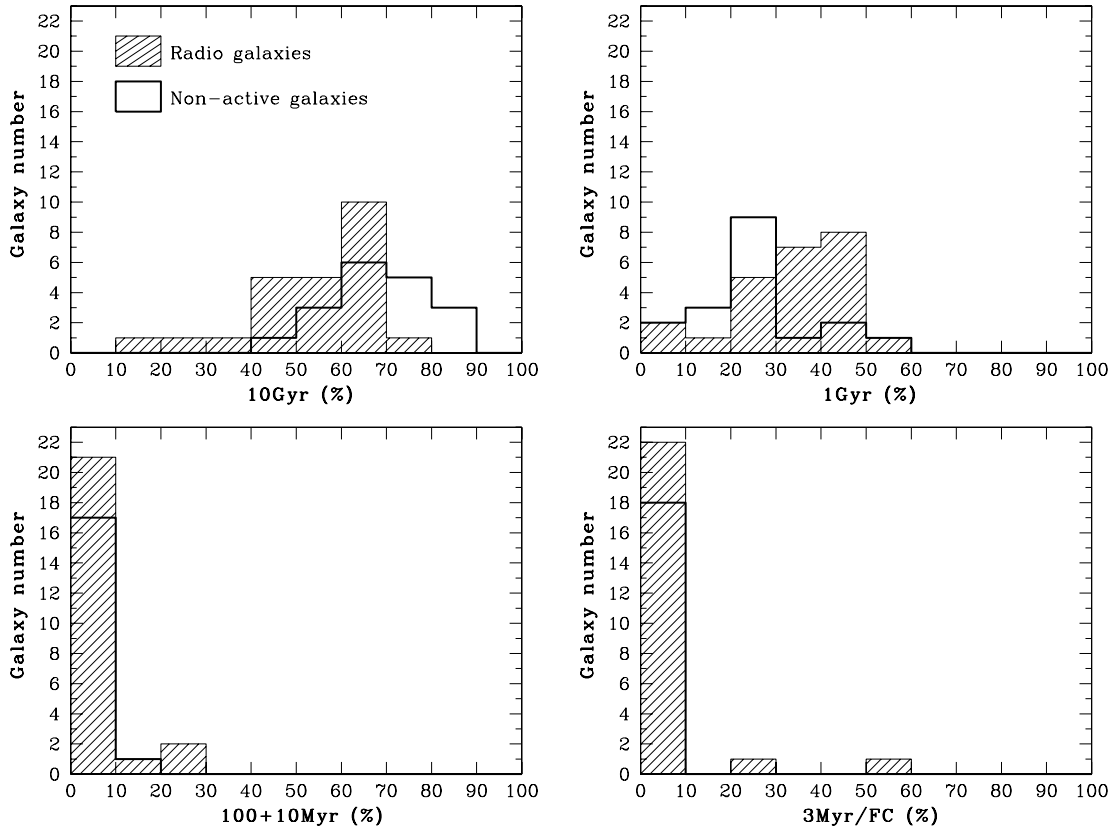

Figure 10. Histograms for the radio and control sample galaxies, comparing the relative contributions of different age components to the total flux at 4020 Å. Open histograms with a heavy outline show the non-active galaxies while hatched histograms show the radio galaxies.

systematically smaller, while the contribution of the 1-Gyr component is systematically larger than in the control sample.

The above results suggest that 1-Gyr-old star formation episodes have been more frequent in radio galaxies than in non-active galaxies of the same Hubble type, suggesting a relation between star formation episodes triggered 1 Gyr ago and the presence of radio activity at the present time. In addition, the correlation between the radio power and the contribution of the 1-Gyr component that we found in the previous section suggests that the radio power is correlated with the mass of the starburst.

6 SUMMARY AND CONCLUSIONS

In this paper we have studied the nuclear and extranuclear stellar populations of a complete sample of 24 radio galaxies and a control sample of 18 non-active early-type galaxies, matched in Hubble type to those of the radio sample. The main conclusions of this work can be summarized as follows.

(i) In most radio galaxies, the stellar population is dominated by old (10 Gyr) and intermediate-age (1 Gyr) components.

(ii) Blue continua due to an AGN and/or to recent star formation episodes (100 Myr old or younger) are found in only four of the 24 radio galaxies. Two of these are BLRGs, for which the blue continuum is probably dominated by the AGN light. The frequency of clear signatures of recent star formation as the dominant source of blue continuum in our complete sample is thus no more than 10–15 per cent. This value is much smaller than the ∼40 per cent frequency that we found in our previous studies of Seyfert 2 galaxies (e.g. Storchi-Bergmann et al. 2000; Raimann et al. 2003, and references therein).

(iii) The four radio galaxies with a significant contribution from young components and/or direct AGN light are all FR II/x. There seems, therefore, to be a systematic difference between FR I and FR II stellar populations, in the sense that FR II radio galaxies have larger contributions from younger stellar populations. A larger sample is needed to better quantify this difference.

(iv) There is an inverse relation between the strength of the emission line [O III] λ5007 and the mean age of the stellar population, suggesting that younger galaxies have more active nuclei.

(v) There is also a relation between the radio power and the mean age of the stellar population in the sense that younger galaxies host more powerful radio sources.

(vi) The main difference between the stellar populations of the radio and control sample galaxies is that the former have, on average, a larger contribution from the intermediate-age 1-Gyr component. This excess contribution suggests a relation between the present radio activity and a past episode of star formation which occurred about 1 Gyr ago.

In order to explain the above results we speculate on an evolutionary scenario for the radio galaxies, similar to the one we have proposed for Seyfert galaxies (Storchi-Bergmann et al. 2000): a past event which occurred more than 10^9 yr ago (e.g. interaction with a passing external galaxy, or merger) has triggered an episode of star formation in the inner region. After an average delay of 10^9 yr the radio activity sets in. Our results also suggest that the more massive the starburst, the stronger the subsequent radio emission.

Comparing the present results for the radio galaxies with those for Seyferts (Storchi-Bergmann et al. 2000), we conclude that while for Seyfert 2 galaxies the delay between the triggering of star formation and the onset of activity would be, on average, 10^8 yr, for the radio galaxies this delay would be an order of magnitude longer.

ACKNOWLEDGMENTS

DR and TSB acknowledge support from the Brazilian Institutions CNPq, CAPES and FAPERGS. RWH acknowledges support from grants awarded by the Australian Research Council. HQ acknowledges partial support from the FONDAP Centro de Astrofisica. We thank the referee for useful suggestions which helped to improve the paper. The NED is operated by the Jet Propulsion Laboratory, California Institute of Technology, under contract with the National Aeronautics and Space Administration.

REFERENCES

Aretxaga I., Terlevich E., Terlevich R. J., Cotter G., Díaz Ángeles I., 2001, MNRAS, 325, 636
Bica E., 1988, A&A, 195, 76
Bica E., Alloin D., 1986, A&A, 162, 21
Bica E., Alloin D., Schmitt H. R., 1994, A&A, 283, 805
Burgess A. M., Hunstead R. W., 1994 in Bicknell G. V., Dopita M. A., Quinn P. J., eds, ASP Conf. Ser. Vol. 54, The First Stromlo Symposium: The Physics of Active Galaxies. Astron. Soc. Pac., San Francisco, p. 359
Burgess A. M., Hunstead R. W. 2005, AJ, submitted
Cid Fernandes R. Jr, Storchi-Bergmann T., Schmitt H., 1998, MNRAS, 297, 579
Cid Fernandes R. Jr, Heckman T., Schmitt H., González Delgado R. M., Storchi-Bergmann T., 2001, ApJ, 558, 81
Fabian A. C., 1989, MNRAS, 238, 41P
Fanaroff B., Riley J., 1974, MNRAS, 167, 31
Lilly S. J., Longair M. S., 1984, MNRAS, 211, 833
McCarthy P. J., van Breugel W., Spinrad H., Djorgovski S., 1987, ApJ, 321, L29
Quintana H., Santos J. F. C. Jr, Dottori H., Bica E., 1990, RevMexA&A, 21 213
Raimann D., 2004, PhD thesis, Universidade Federal do Rio Grande do Sul
Raimann D., Storchi-Bergmann T., Bica E., Alloin D., 2001, MNRAS, 324, 1087
Raimann D., Storchi-Bergmann T., González Delgado R. M., Cid Fernandes R., Heckman T., Leitherer C., Schmitt H., 2003, MNRAS, 339, 772
Rees M. J., 1989, MNRAS, 239, 1P
Schmitt H., Storchi-Bergmann T., Cid Fernandes R. Jr, 1999, MNRAS, 303, 173
Storchi-Bergmann T., Raimann D., Bica E. L. D., Fraquelli H. A., 2000, ApJ, 544, 747
Tadhunter C. N., Fosbury R. A. E., di Serego Alighieri S., 1989 in Maraschi L., Maccacaro T., Ulrich M.-H., eds, BL Lac objects. Springer-Verlag, Berlin, p. 79
Tadhunter C., Dickson R., Shaw M. A., 1996, MNRAS, 281, 591
Tadhunter C., Dickson R., Morganti R., Robinson T. G., Wills K., Villar-Martin M., Hughes M., 2002, MNRAS, 330, 977
Wills K. A., Tadhunter C. N., Robinson T. G., Morganti R., 2002, MNRAS, 333, 211
Wills K. A., Morganti R., Tadhunter C. N., Robinson T. G., Villar-Martin M., 2004, MNRAS, 347, 771

This paper has been typeset from a TEX/LATEX file prepared by the author.